IEEE Access
Multidisciplinary | Rapid Review | Open Access Journal

Received May 2, 2020, accepted May 20, 2020, date of publication May 25, 2020, date of current version June 9, 2020.

Digital Object Identifier 10.1109/ACCESS.2020.2997316

Filtered OFDM: An Insight Into Intrinsic In-Band Interference and Filter Frequency Response Selectivity

JUQUAN MAO[1], LEI ZHANG[2], (Senior Member, IEEE), PEI XIAO[1], (Senior Member, IEEE), AND KONSTANTINOS NIKITOPOULOS[1], (Senior Member, IEEE)

[1]Institute for Communication Systems (ICS), Home of 5G Innovation Centre, University of Surrey, Guildford GU2 7XH, U.K.
[2]James Watt School of Engineering, University of Glasgow, Glasgow G12 8QQ, U.K.

Corresponding author: Lei Zhang (lei.zhang@glasgow.ac.uk)

This work was supported in part by the U.K. Engineering and Physical Sciences Research Council under Grant EP/R001588/1, and in part by the University of Surrey 5GIC (http://www.surrey.ac.uk/5gic) members for this work.

ABSTRACT The future mobile networks will face challenges in support of heterogeneous services over a unified physical layer, calling for a waveform with good frequency localization. Filtered orthogonal frequency division multiplexing (f-OFDM), as a representative subband filtered waveform, can be employed to improve the spectrum localization of orthogonal frequency-division multiplexing (OFDM) signal. However, the applied filtering operations will impact the performance in various aspects, especially for narrow subband cases. Unlike existing studies which mainly focus its benefits, this paper investigates two negative consequences inflicted on single subband f-OFDM systems: in-band interference and filter frequency response (FFR) selectivity. The exact-form expression for the in-band interference is derived, and the effect of FFR selectivity is analyzed for both single antenna and multiple antenna cases. The in-band interference-free and nearly-free conditions for f-OFDM systems are studied. A low-complexity block-wise parallel interference cancellation (BwPIC) algorithm and a pre-equalizer are proposed to tackle the two issues caused by the filtering operations, respectively. Numerical results show that narrower subbands suffer more performance degradation compared to wider bands. In addition, the proposed BwPIC algorithm effectively suppresses interference, and pre-equalized f-OFDM (pf-OFDM) considerably outperforms f-OFDM in both single antenna and multi-antenna systems.

INDEX TERMS Filtered OFDM, frequency response selectivity, in-band interference, interference cancellation.

I. INTRODUCTION

Orthogonal frequency-division multiplexing (OFDM) has strengths such as robustness against multi-path fading, a simple implementation based on fast Fourier transform (FFT) algorithms, and perfect compatibility with multiple-input-multiple-output (MIMO) technique, and so on. With these advantages, OFDM is extensively adopted in modern communication systems. However, due to limited spectrum localization, OFDM has significant limitations in challenging new spectrum use scenarios, such as asynchronous multiple access, as well as mixed numerology cases aiming to use adjustable numerologies, such as subcarrier spacing (SCS), symbol length, and cyclic prefix (CP) length, in support of diverse service requirements [1], [2].

To address the mentioned limitations of OFDM, several candidate waveforms and their variants, such as filter bank multicarrier (FBMC) [3], [4], generalized frequency division multiplexing (GFDM) [5], [6], universal filtered multicarrier (UFMC) [7] are being studied and promoted. The comparisons among these schemes with respects to different criteria can be found in [2], [8], [9]. Regarding OFDM based advanced waveform candidates, filtered OFDM (f-OFDM) schemes are receiving considerable attention due to their ability to address the mentioned issues while maintaining a high level of commonality with legacy OFDM systems [10], [11]. Specifically, the system bandwidth is divided into arbitrary numbers of subbands, each containing a legacy OFDM signal.

The associate editor coordinating the review of this manuscript and approving it for publication was Mostafa Zaman Chowdhury.

This work is licensed under a Creative Commons Attribution 4.0 License. For more information, see https://creativecommons.org/licenses/by/4.0/

Consequently, f-OFDM is capable of retaining the advantages of OFDM while avoiding its limitations. First, filtering is applied to every single subband to suppress OOB emissions;[1] thus the guard band can be reduced with a better-localized spectrum. Second, numerology can be optimized independently for a certain type of service within each subband; thus services with different technical requirements are flexibly supported. Third, thanks to the filtering, the synchronization requirement is also relaxed due to the reduced sidelobe, making interference from asynchronous transmissions more tolerable.

Many aspects of f-OFDM, such as general framework and methodology, design and implementation, and field trials, have been reported in literature [10]–[18]. However, much of the research up to now has studied the advantages [10], [11], [14], and there is a lack of mathematical analysis on the negative consequences brought by filtering operations, for instance, in-band interference and filter frequency response (FFR) selectivity. Zhang *et al.* progressed further by deriving a system model in [19] to quantitatively analyze interference in f-OFDM systems, in which the channel matrix is divided into three parts to decompose total inferences into inter-symbol interference (ISI) and adjacent carrier interference (ACI). The limitation of this method is that it can neither differentiate the interference induced by channel or filtering nor the inter-carrier interference from other subbands or its own band. To better suppress OOB emissions, the filters employed in f-OFDM systems are usually very long (up to half of FFT size [11], [13]), which inevitably leaves the systems prone to in-band interference. The existing works in the literature indicate that it has a trivial influence on system performance for medium to wide subbands [17], [18], and few studies have investigated the performance degradation in narrow subband systems. FFR selectivity refers to non-uniform filter frequency response in a transition band, which reduces the power of signals on the corresponding subcarriers and makes them undesirable for carrying data. As a result, the system bandwidth efficiency can be compromised significantly, especially in the case of narrower subbands. Although existing works [20], [21] have discussed the FFR selectivity in a single-antenna case, to the best of our knowledge, no studies have investigated the issue in the multi-antenna scenario.

In our paper, we aim to fill the above-mentioned gaps and contribute as follows:

- We develop an analytical model for 3GPP-compatible single band f-OFDM systems, in which the receiver has no knowledge of the transmitter filter [22]. Based on the model, the in-band interference signal is decomposed into ICI, forward ISI, and backward ISI, such that the impact of each interference component can be studied individually.
- An analytical metric to quantify the interference level is developed as a function of several system parameters. This work leads to the derivation of the condition for in-band interference-free systems, and provides the practical approach for the selection of cyclic redundancy length to balance system efficiency and receiver complexity. A novel low-complexity block-based parallel interference cancellation algorithm is then proposed for the in-band interference mitigation.
- The system performance degradation exerted by FFR selectivity is first analyzed in single antenna f-OFDM systems. The results are extended to the multi-antenna f-OFDM case, and a system model for analyzing spatial orthogonality in multi-antenna SFBC-f-OFDM systems is developed. The spatial orthogonality is proved to be no longer valid, and the analytical expression of spatial interference power is derived. A pre-equalizer is proposed at the transmitter to alleviate the adverse effect at the cost of subband bandwidth-dependent power loss.
- Simulations are carried out for evaluating the performance of f-OFDM with different settings in subband width so that the performance of narrow subbands is studied in comparison with wide subbands.

The rest of the paper is organized as follows: Section II presents the single subband f-OFDM transceiver structure and describes the system model. Section III analyzes the in-band interference and introduces approaches to suppress the interference. Section IV focuses on the discussion of the impact of FFR selectivity on both single-antenna and multi-antenna systems. Section V presents numerical results. Finally, Section VI concludes the paper.

Notations: $\mathcal{E}\{\cdot\}$ denotes the expectation operator. Vectors and matrices are denoted by boldface lower-case and upper-case characters, and the operators $(\cdot)^*$, $(\cdot)^T$ and $(\cdot)^H$ represent complex conjugate, transpose, and conjugate transpose, respectively. The $M \times M$ identity matrix is denoted by $\mathbf{I}_M$. diag($\mathbf{x}$) is a function returning a square diagonal matrix with the elements of vector $\mathbf{x}$ on the main diagonal, while diag($\mathbf{A}$) returns a column vector of the main diagonal elements of matrix $\mathbf{A}$. $|\cdot|$ denotes the magnitude of a complex number, while $\|\cdot\|$ is the Frobenius norm of a matrix. $.*$ denotes the element-wise multiplication, $\mathbb{R}$ and $\mathbb{C}$ represent real and complex space, respectively.

II. SYSTEM MODEL FOR f-OFDM SISO SYSTEM

In this section, we describe a system model for single band f-OFDM systems in which the interference (including ICI, forward ISI, and backward ISI) induced by filtering operations are investigated. These interference components are referred as in-band interference in the paper. The interference from the other subbands in the system (inter-subband interference) is out of the scope of our work.[2] Assume M

[1] In general, the filtering is only needed between the subbands of different numerologies (or asynchronous transmissions). In this paper, we assume each subband is with a different numerology.

[2] Interested users are referred to [23], which gives a thorough analysis on inter-subband interference.

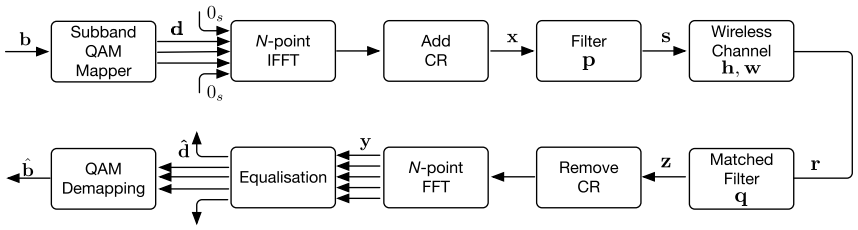

FIGURE 1. Block diagram of the f-OFDM transceiver.

consecutive subcarriers in the range of $\mathcal{M} = \{M_0, M_0 + 1, \ldots, M_0 + M - 1\}$ are assigned to the subband with a corresponding waveform shaping filter denoted as vector $\mathbf{p}$ in the time domain and $\ddot{\mathbf{p}}$ in the frequency domain.

Considering the block diagram depicted in Fig. 1, a sequence of information bits $\mathbf{b}$ is fed into a quadrature amplitude modulation (QAM) mapper to obtain symbols from a 2^{μ}-valued complex constellation, where μ is the modulation order. Representing the complex symbols in K consecutive OFDM symbols in a sub-frame as a length MK vector gives

$$\mathbf{d} = [\mathbf{d}_0^T, \mathbf{d}_1^T, \ldots, \mathbf{d}_{K-1}^T]^T \tag{1}$$

where $\mathbf{d}_k = [d_{k,0}, d_{k,1}, \ldots, d_{k,M-1}]^T \in \mathbb{C}^{M\times 1}$ with the individual element $d_{k,m}$ corresponding to the data symbol transmitted on the m-th subcarrier in the k-th OFDM symbol. The data symbols contained in $\mathbf{d}_k$ are assumed to be independent and identically distributed (i.i.d.) with $\mathcal{E}\{\mathbf{d}_k \mathbf{d}_k^H\} = \sigma_s^2 \mathbf{I}$, where σ_s^2 is average transmission power of QAM symbols.

The transmitter and receiver procedures are described as follows:

1) **Inverse fast Fourier transform (FFT) and cyclic redundancy (CR) appending**. An N-point ($N > M$) inverse FFT operation is performed on per OFDM symbol basis, followed by an addition of a CR of length N_{cr} for eliminating/mitigating ISIs. The CR is made up of two parts, cyclic prefix (CP) of length N_{cp} and cyclic suffix (CS) of length N_{cs} ($N_{\text{cr}} = N_{\text{cp}} + N_{\text{cs}}$). To be compatible with CP-OFDM, CR can be implemented as an extended CP which incorporates CP and CS at the transmitter, and the FFT window at the receiver is moved forward by the length of CS. The CP is adopted for combating the ISI induced by the dispersive nature of channels and the ISI introduced by filter forward spreading, while the CS focuses on the alleviation of the ISI induced by the filter backward spreading. The k-th OFDM symbol can be expressed in the form of matrix multiplication as

$$\mathbf{x}_k = \rho_{\text{cr}} \mathbf{T}_{\text{cr}} \mathbf{F} \mathbf{d}_k \in \mathbb{C}^{L\times 1}, \tag{2}$$

where $\mathbf{x}_k$ is a vector of dimension $L = N + N_{\text{cr}}$. $\mathbf{F}$ is an $N \times M$ submatrix of N-point IFFT matrix defined by its element on the n-th row and m-th column as $F_{n,m} = 1/N \exp\{\frac{j2\pi n(m+M_0)}{N}\}$, and it is unitary as $\mathbf{F}^H\mathbf{F} = \mathbf{I}_M$. $\mathbf{T}_{\text{cr}} = [\mathbf{I}_{\text{cp}}^T, \mathbf{I}_N, \mathbf{I}_{\text{cs}}^T]^T$ is the $L \times N$ matrix inserting the CP and CS, with $\mathbf{I}_{\text{cp}}$ and $\mathbf{I}_{\text{cs}}$ containing the last and the first N_{cp} rows of the identity matrix $\mathbf{I}_N$, respectively. ρ_{cr} is the power normalization factor defined as $\rho_{\text{cr}} = \sqrt{N/L}$.

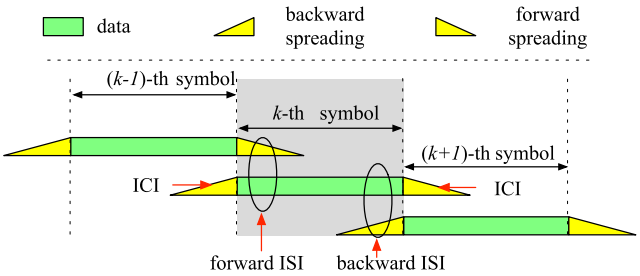

FIGURE 2. f-OFDM filtering illustration.

2) **Transmitter filtering**. By applying a spectrum shaping filter, the actual transmitted f-OFDM signal is obtained as

$$\mathbf{s} = \mathbf{x} * \mathbf{p}, \tag{3}$$

where $\mathbf{x} = [\mathbf{x}_0, \mathbf{x}_1, \ldots, \mathbf{x}_{K-1}]^T$, and

$$\mathbf{p} = [p_0, p_1, \ldots, p_{N_p}]^T \tag{4}$$

is a length $N_p + 1$ vector describing the impulse response of the transmit filter. The filter is designed to be centered in the assigned subband with a width equivalent to the bandwidth of the subband. N_p is typically chosen to ensure the signal dispersion due to the transmitter and receiver filtering under one f-OFDM symbol duration, such that the f-OFDM symbol of interest only suffers ISI from its direct neighbors.

The signal spreads bi-directionally and inflicts interference between adjacent OFDM symbols. The forward/backward ISI are generated by the forward/backward spreading of the previous/next OFDM symbols to the current symbol window [11]. While the ICI comes from the energy loss of the current OFDM symbol due to its bi-directional spreading. More specifically, as illustrated in Fig. 2, the forward ISI to the k-th OFDM symbol comes from the forward spreading of the (k-1)-th OFDM symbol, i.e., the yellow triangle pointing to the right and overlapped with k-th OFDM symbol in green. The backward ISI to the k-th OFDM symbol comes from the backward spreading of the $(k + 1)$-th OFDM symbol, i.e., the yellow triangle pointing to the left and overlapped with k-th OFDM symbol. The ICI to the k-th OFDM symbol is caused by the backward/forward spreading of itself, i.e., the two yellow triangles connected to the k-th OFDM symbol representing information lost to the k-th OFDM symbol.

To facilitate the interference analysis caused by filtering, we derive the equivalent matrix form of a linear filtering process. The L received samples relative to the k-th OFDM symbol are grouped in the vector $\mathbf{s}_k$, thus obtaining

$$\mathbf{s}_k = \mathbf{P}^u \mathbf{x}_{k-1} + \mathbf{P}^m \mathbf{x}_k + \mathbf{P}^l \mathbf{x}_{k+1}, \tag{5}$$

where the $L \times L$ matrix $\mathbf{P}^u$ spreads the $(k-1)$-th OFDM symbol into the core window of the k-th OFDM symbol and causes the forward ISI. It is a strictly upper triangular matrix defined by its (i, j)-th element as

$$P^u{}_{i,j} = \begin{cases} p_{\frac{N_p}{2}+L+i-j}, & j \geq i + L - \dfrac{N_p}{2} \\ 0, & j < i + L - \dfrac{N_p}{2}. \end{cases} \tag{6}$$

The matrix $\mathbf{P}^m$ is a Toeplitz matrix specified by its first column $\left[p_{\frac{N_p}{2}}, \ldots, p_{N_p}, \mathbf{0}_{1\times(L-\frac{N_p}{2}-1)}\right]^T$ and first row $\left[p_{\frac{N_p}{2}}, \ldots, p_0, \mathbf{0}_{1\times(L-\frac{N_p}{2}-1)}\right]^T$. It is a matrix in which all nonzero entries are on the main diagonal and the first $\frac{N_p}{2}$ diagonals above and below.

The matrix $\mathbf{P}^l$ extends the $(k+1)$-th OFDM symbol into the core window of the k-th OFDM symbol and leads to the backward ISI. It is a strictly lower triangular matrix defined by its (i, j)-th element

$$P^l{}_{i,j} = \begin{cases} p_{\frac{N_p}{2}-1-L+i-j}, & i \geq j + L - \dfrac{N_p}{2} + 1 \\ 0, & i < j + L - \dfrac{N_p}{2} + 1. \end{cases} \tag{7}$$

3) **Passing the channel**. An $(N_{\text{ch}}+1)$-tap ($N_{\text{ch}} \leq N_{\text{cp}}$) channel is assumed to have an impulse response

$$\mathbf{h} = [h_0, h_1, \ldots, h_{N_{\text{ch}}}]^T. \tag{8}$$

After passing the above channel followed by an addition of additive white Gaussian noise (AWGN), the L received samples corresponding to the k-th OFDM symbol can be written as

$$\mathbf{r}_k = \mathbf{H}^u \mathbf{s}_{k-1} + \mathbf{H}^m \mathbf{s}_k + \mathbf{w}_k, \tag{9}$$

where $\mathbf{H}^m$ is a Toeplitz matrix with $[\mathbf{h}^T, \mathbf{0}_{1\times(L-N_{\text{ch}}-1)}]^T \in \mathbb{C}^{L\times 1}$ as its first column and $[h_0, \mathbf{0}_{1\times(L-1)}]^T \in \mathbb{C}^{L\times 1}$ as its first row.

$\mathbf{H}^u$ is the matrix relative to the channel spreading, and it is a strictly upper triangular matrix defined by its (i, j)-th element as

$$H^u{}_{i,j} = \begin{cases} h_{L+i-j}, & j \geq i + L - N_{\text{ch}} \\ 0, & \text{otherwise.} \end{cases} \tag{10}$$

$\mathbf{w}_k$ is the Gaussian noise vector with each element having zero mean and variance σ_n^2.

4) **Filtering at the receiver side**. 3GPP suggests that spectral confinement techniques, such as filtering or windowing for a waveform at the transmitter, should be transparent to the receiver [22]. Therefore, we assume that the receiver has no knowledge of the transmitter filtering and define a length $N_q + 1$ receiver filter as

$$\mathbf{q} = [q_0, q_1, \ldots, p_{N_q}]^T. \tag{11}$$

The L samples corresponding to the k-th OFDM symbol passing through the receiver filter are grouped into the vector $\mathbf{z}_k$, obtaining

$$\mathbf{z}_k = \mathbf{Q}^u \mathbf{r}_{k-1} + \mathbf{Q}^m \mathbf{r}_k + \mathbf{Q}^l \mathbf{r}_{k+1}, \tag{12}$$

where $\mathbf{Q}^u$, $\mathbf{Q}^m$, $\mathbf{Q}^l$ are all $L \times L$ matrices defined in a similar approach as $\mathbf{P}^u$, $\mathbf{P}^m$, $\mathbf{P}^l$, respectively. Their definitions are omitted to conserve space.

After some basic algebraic manipulations, $\mathbf{z}_k$ can be expressed as

$$\mathbf{z}_k = \Theta_{\text{pre}} \mathbf{x}_{k-1} + \Theta \mathbf{x}_k + \Theta_{\text{next}} \mathbf{x}_{k+1} + \tilde{\mathbf{w}}_k, \tag{13}$$

where the definitions of Θ_{pre}, Θ, Θ_{next}, and $\tilde{\mathbf{w}}_k$ can be found in Appendix A.

5) **Equalization and detection.** By applying matrix $\mathbf{R}_{\text{cr}} = [\mathbf{0}_{N\times N_{\text{cp}}}, \mathbf{I}_N, \mathbf{0}_{N\times N_{\text{cs}}}] \in \mathbb{B}^{N\times L}$ to $\mathbf{z}_k$ in (46), the CR is removed. After FFT at the receiver, we obtain $\mathbf{y}_k = \mathbf{F}^H \tilde{\mathbf{y}}_k = \mathbf{F}^H \mathbf{R}_{\text{cr}} \mathbf{z}_k$, which can be rearranged based on (13) and (2) as

$$\mathbf{y}_k = \Psi_{\text{pre}} \mathbf{d}_{k-1} + \Psi \mathbf{d}_k + \Psi_{\text{next}} \mathbf{d}_{k+1} + \hat{\mathbf{w}}_k, \tag{14}$$

where $\Psi_{\text{pre}} = \rho_{\text{cr}} \mathbf{F}^H \mathbf{R}_{\text{cr}} \Theta_{\text{pre}} \mathbf{T}_{\text{cr}} \mathbf{F}$ is the $M \times M$ matrix that produces forward ISI, while $\Psi_{\text{next}} = \rho_{\text{cr}} \mathbf{F}^H \mathbf{R}_{\text{cr}} \Theta_{\text{next}} \mathbf{T}_{\text{cr}} \mathbf{F}$ produces backward ISI, and $\hat{\mathbf{w}}_k = \mathbf{F}^H \mathbf{R}_{\text{cr}} \tilde{\mathbf{w}}_k$ is the Fourier transformed AWGN vector. $\Psi = \rho_{\text{cr}} \mathbf{F}^H \mathbf{R}_{\text{cr}} \Theta \mathbf{T}_{\text{cr}} \mathbf{F}$ is a $M \times M$ matrix transforming the desired signal. It is generally not a strict diagonal matrix unless $N_{\text{cr}} > N_p + N_q + N_{\text{ch}}$ (will be discussed in detail in Section III-A). We decompose Ψ into a diagonal matrix $\Psi_\Lambda = \text{diag}(\text{diag}(\Psi))$ and another matrix Ψ_e as $\Psi = \Psi_\Lambda + \Psi_e$. The $M \times M$ matrix Ψ_e with all its diagonal elements being zero, and its non-diagonal elements, copied from the same positions of the matrix Ψ, produces the ICI. By substituting Ψ with $\Psi_\Lambda + \Psi_e$, (14) can be rearranged as

$$\mathbf{y}_k = \underbrace{\Psi_\Lambda \mathbf{d}_k}_{\text{desired signal}} + \underbrace{\Psi_e \mathbf{d}_k}_{\text{ICI}} + \underbrace{\Psi_{\text{pre}} \mathbf{d}_{k-1}}_{\text{forward ISI}} + \underbrace{\Psi_{\text{next}} \mathbf{d}_{k+1}}_{\text{backward ISI}} + \underbrace{\hat{\mathbf{w}}_k}_{\text{noise}}. \tag{15}$$

5) *Equalization and Detection:* The signal expressed in (15) can be equalized using the classic equalization methods with a trade-off between complexity and performance. The simplest method is one-tap equalization using diagonal matrix Ψ_Λ, obtained as $\hat{\mathbf{d}}_k = \Psi_\Lambda^{-1} \mathbf{y}_k$, which can be conducted independently on each subcarrier. However, one-tap equalization can only achieve sub-optimal performance due to the ignored intrinsic interference. More advanced equalization methods will be discussed in Section III-D.

III. IN-BAND INTERFERENCE ANALYSIS AND DISCUSSION

A. CHANNEL DIAGONALIZATION AND IN-BAND INTERFERENCE-FREE SYSTEMS

In interference-free systems, the channel can be fully diagonalized so that the elegant one-tap equalization can be utilized

to achieve optimal performance. In the sequel, we will derive the condition to achieve interference-free f-OFDM systems. The in-band interference signal to the k-th f-OFDM symbol can be decomposed into three components based on (15) as

$$\mathbf{I}_k = \underbrace{\Psi_e \mathbf{d}_k}_{\text{ICI}} + \underbrace{\Psi_{\text{pre}} \mathbf{d}_{k-1}}_{\text{forward ISI}} + \underbrace{\Psi_{\text{post}} \mathbf{d}_{k+1}}_{\text{backward ISI}}. \tag{16}$$

The matrix Ψ_{pre} produces the filtering/channel forward ISI. It is a strictly upper triangular matrix, of which only the top $N_p + N_{\text{ch}}$ rows have non-zero elements. The proof can be found in Appendix B. When $\mathbf{R}_{\text{cr}}$ is applied to remove the non-zero rows of Θ_{pre}, the length of CP can be chosen as

$$N_{\text{cp}} \geq N_p + N_{\text{ch}} \tag{17}$$

to force a zero-valued Ψ_{pre} such that zero forward ISI is ensured.

The matrix Ψ_{next} generates the filtering backward ISI. It is a strict lower triangular matrix of which only the bottom N_q rows have non-zero elements. The proof is omitted to conserve space since it can be easily done in a similar fashion to Θ_{pre}. Similarly, the length of CS can be chosen as

$$N_{\text{cs}} \geq N_q \tag{18}$$

to secure a zero backward ISI.

When (17) and (18) are met, the adding cyclic redundancy converts the linear convolution $\mathbf{q} * \mathbf{h} * \mathbf{p} * \mathbf{x}$ into a circular convolution $\mathbf{q} \circledast \mathbf{h} \circledast \mathbf{p} \circledast \mathbf{x}$. From the definition of convolution theorem, circular convolution in the time domain leads to multiplication in the frequency domain. Denote $\ddot{\mathbf{p}}, \ddot{\mathbf{h}}, \ddot{\mathbf{q}}$ as DFT of $\mathbf{p}, \mathbf{h}, \mathbf{q}$ in the subband, the received data symbol vector $\mathbf{y}_k$ in (14) can be reformed as

$$\mathbf{y}_k = \mathbf{\Lambda} \mathbf{d}_k + \hat{\mathbf{w}}_k, \tag{19}$$

where the $M \times M$ diagonal matrix $\mathbf{\Lambda} = \mathbf{QHP}$ with $\mathbf{Q} = \text{diag}(\ddot{\mathbf{q}})$, $\mathbf{H} = \text{diag}(\ddot{\mathbf{h}})$, $\mathbf{P} = \text{diag}(\ddot{\mathbf{p}})$.

The equation (19) implies that $\Psi = \Psi_\Lambda = \mathbf{\Lambda}$ and the ICI generating matrix $\Psi_e = 0$. Thus, zero in-band ICI is guaranteed.

With the discussion above, we form the following Proposition:

Proposition 1: Consider a single-band f-OFDM system depicted in Fig. 1 with the transmitter, the channel, and the receiver filter being defined in (4),(8),(11). It is an in-band interference-free system under the condition of perfect synchronization at the receiver if

$$N_{\text{cp}} \geq N_p + N_{\text{ch}} \quad \text{and } N_{\text{cs}} \geq N_q, \tag{20}$$

and the received data symbol can be expressed as in (19).

B. IN-BAND INTERFERENCE POWER

When the interference-free condition in (20) is violated, i.e., $N_{\text{cp}} < N_p + N_{\text{ch}}$ or $N_{\text{cs}} < N_q$, the system will not be strictly orthogonal. In the time domain, the signal from adjacent OFDM symbols spreads into the core window of the OFDM symbol of interest, which produces the forward and backward ISI. In the frequency domain, the extended part of the interested OFDM symbol falls out the range of CP/CS and leads to the energy lost. As a result, the matrix Ψ is no longer diagonal, causing the ICI. The average power of the desired signal and interference signal including forward ISI (f-ISI), backward ISI (b-ISI), and ICI on all subcarriers in one transmission block can be grouped as an $N \times 1$ vector, obtained as

$$\begin{aligned} \boldsymbol{\eta}_x = {} & \mathcal{E}\{\text{diag}(\Psi_x \Psi_x^H)\}\sigma_s^2 \\ & (\boldsymbol{\eta}_x, \Psi_x) \in \{(\boldsymbol{\eta}_s, \Psi_\Lambda), (\boldsymbol{\eta}_{\text{f-ISI}}, \Psi_{\text{pre}}), \\ & (\boldsymbol{\eta}_{\text{b-ISI}}, \Psi_{\text{next}}), (\boldsymbol{\eta}_{\text{ICI}}, \Psi_e)\}. \end{aligned} \tag{21}$$

Forcing the channel matrix to be an identity channel ($N_{\text{ch}} = 1, \mathbf{H}^m = 1, \mathbf{H}^u = 0$), so that the interference induced by the channel can be avoided, and the interference signal from filtering itself can be studied. The average power of the aforementioned signal can be rearranged as

$$\begin{aligned} \boldsymbol{\eta}_x = {} & \text{diag}(\Psi_x \Psi_x^H)\sigma_s^2 \\ & (\boldsymbol{\eta}_x, \Psi_x) \in \{(\boldsymbol{\eta}_s, \Psi_\Lambda), (\boldsymbol{\eta}_{\text{f-ISI}}, \Psi_{\text{pre}}), \\ & (\boldsymbol{\eta}_{\text{b-ISI}}, \Psi_{\text{next}}), (\boldsymbol{\eta}_{\text{ICI}}, \Psi_e)\}. \end{aligned} \tag{22}$$

The system signal to interference plus noise ratio (SINR) can then be calculated as

$$\boldsymbol{\gamma} = \frac{\boldsymbol{\eta}_s}{\sum_{x \in \{\text{f-ISI,b-ISI,ICI}\}} \boldsymbol{\eta}_x + \text{diag}(\hat{\mathbf{w}}_k \hat{\mathbf{w}}_k^H)}. \tag{23}$$

With the provided SINR, some existing works, such as [24], [25], are available for calculating system BER under various channels and different modulation/coding schemes. Due to the page limitation, we will not expand this part in the work but consider it as a possible usage of our derivations and leave it to our future work.

C. IN-BAND INTERFERENCE MITIGATION: A PRACTICAL APPROACH FOR CHOOSING CR LENGTH

Proposition 1 implies that in-band interference-free systems can be achieved by adding a sufficient number of redundant samples. The implementation of CR, although elegant and simple, is not entirely free. It comes with a bandwidth and power penalty. Since N_{cr} redundant samples are transmitted, the actual bandwidth for f-OFDM increases from B to $\frac{N_{\text{cr}}+N}{N}B$. Similarly, an additional N_{cr} samples must be counted against the transmit power budget resulting in a power loss of $10 \log_{10} \frac{N_{\text{cr}}+N}{N}$ dB. For an f-OFDM system with stringent frequency localization requirement, the filter length can be chosen up to half of the symbol duration, making the satisfaction of interference-free condition in (20) unaffordable with respect to the power and bandwidth loss. On the one hand, interference-free systems are preferred due to the benefit to the computational complexity reduction and the SINR improvement. On the other hand, a highly efficient system requires shorter overhead (CP/CS). Therefore, choosing the size of CR, as a tradeoff between the two contradicting parties, forms an optimization problem. However, it is very

hard to find an optimal solution due to the multi-objective characteristic of the problem.

A sub-optimal attempt in the literature [10] is suggested by setting the length of overhead to the width of the main lobe, due to the fact that the main lobe of a sinc filter carries most of its energy. However, it neglects the fact that filters of different bandwidth vary in energies captured by the main lobes. For instance, a wider subband filter has less energy enclosed in the main lobe. We take this into consideration and propose a subband width-dependent approach for choosing the CR length.

For a length $K+1$ filter defined as $\mathbf{f} = [f_0, f_1 \ldots, f_K]^T$, occupying a subband of width equivalent to M subcarriers in a channel of N subcarriers, the energy rate consisting in the k middle samples is defined as

$$\zeta(\mathbf{f}, k) = \frac{\sum_{m=\frac{K}{2}-\frac{k}{2}}^{\frac{K}{2}+\frac{k}{2}} f_m f_m^*}{\sum_{m=0}^{K} f_m f_m^*} \tag{24}$$

Then, the number of overhead can be chosen to ensure that the minimum energy captured by the cyclic redundancy is greater than a pre-defined value. We define the following proposition:

Proposition 2: Consider a single-band f-OFDM system depicted in Fig. 1 with the transmitter filter, the channel and the receiver filter being defined in (4), (8), and (11), respectively. It is considered as a nearly in-band interference-free system under the condition of perfect synchronization at the receiver if

$$N_{\text{cp}} \geq K_p + N_{\text{ch}} \quad \text{and } N_{\text{cs}} \geq K_q, \tag{25}$$

where K_p and K_q are selected to satisfy

$$\arg\min_{K_p} \zeta(\mathbf{p}, K_p) \geq \alpha \quad \text{and} \quad \arg\min_{K_q} \zeta(\mathbf{q}, K_q) \geq \alpha \tag{26}$$

with α being a pre-defined value, e.g., $\alpha = 0.99$. The received data symbol can then be approximated by (19) with trivial interference small enough to be ignored, and the effective channel is nearly diagonal.[3]

When the condition in (25) is met, it can be seen from the numerical results in Fig. 8 that the power of effective interference, i.e., the maximum total power of ICI, forward ISI, backward ISI, reduces to the level very close to -30 dB. Eq. (25) is named as a nearly in-band interference-free condition of f-OFDM systems.

The solutions to the optimization problems in (26) can be obtained using a linear search in a sorted list $(1, 2, \ldots, K)$. In particular, the linear search sequentially checks each element of the list and evaluates ζ in (24) until it finds the first CP length that satisfies the specified condition in (26). The denominator of ζ is a constant value (only calculated once), and the numerator is a accumulated term. Therefore, the calculation of ζ at each iteration comprises an addition, a multiplication, and a division, i.e., the computation complexity of each iteration is constant. In the worst cases, it makes K comparisons. however, the optimal CP length can be found close to the width of the first main lob ($\lfloor N/M \rfloor$) due to the energy distribution nature of the filter. Therefore, the complexity of the search algorithm is $\mathcal{O}(N/M)$.

[3]How close the effective channel to a diagonal matrix can be measured quantitatively by Frobenius norm of the matrix Ψ_e. The smaller the $||\Psi_e||_F$ is, the closer the effective channel is equivalent to a diagonal matrix. $||\Psi_e||_F = 0$ indicates a perfect diagonal matrix.

D. AN ALTERNATIVE FOR IN-BAND INTERFERENCE MITIGATION: FREQUENCY EQUALIZATION (FEQ)

1) LINEAR EQUALIZERS

Two representative equalizers, i.e., zero-forcing (ZF) and minimum mean squared error (MMSE), apply an equalization matrix to the current symbol to reverse the effective channel effect. Considering that the received signal of the k-th f-OFDM symbol can be expressed as

$$\mathbf{y}_k = \Psi \mathbf{d}_k + \text{interference terms} + \hat{\mathbf{w}}_k, \tag{27}$$

we define ZF and MMSE equalizers in f-OFDM systems as

$$\begin{aligned} \mathbf{E}_{\text{eq}}^{\text{zf}} &= (\Psi \Psi^H)^{-1} \Psi^H, \\ \mathbf{E}_{\text{eq}}^{\text{mmse}} &= \Psi^H (\Psi \Psi^H + \sigma_n^2 \mathbf{I})^{-1}. \end{aligned} \tag{28}$$

2) NON-LINEAR EQUALIZERS

A non-linear equalizer has improved performance relative to linear receivers by employing interference cancellation (IC) techniques [26]. Generally, IC schemes are implemented in an iterative manner, where the unwanted signal decoded from the previous round is subtracted from the received signal, which in turn is used for decoding the desired signal in the current round. IC can be performed in parallel (PIC), when the contribution of all interfering signal is canceled simultaneously, or in sequence (SIC), when the contribution of the strongest remaining interferer is canceled iteratively. In general, SIC outperforms PIC but comes with high computational complexity due to its high cancellation granularity. However, when the interferes have no significant difference in distortion level, PIC is preferred because it has a comparable performance but a lower computational complexity comparing to its counterpart [27]. The time symmetry property of filters implies that PIC is a better choice for in-band interference mitigation in f-OFDM systems.

We propose a novel PIC algorithm customized for f-OFDM systems, namely, block-wise parallel interference cancellation (BwPIC). It only performs cancellation once for all f-OFDM symbols in a data block per iteration. The algorithm comes with a lower complexity because the number of cancellation operations is reduced by a factor of K comparing to SIC, where K refers to the number of OFDM symbols in one data block.

The algorithm cancels the in-band interference of all f-OFDM symbols in one block in parallel. The detail is shown in Algorithm 1. It involves a sequence of interference cancellation/equalization/slicing operations. At each iteration of the outer loop, a vector $\tilde{\mathbf{d}} = [\tilde{\mathbf{d}}_0, \ldots, \tilde{\mathbf{d}}_{K-1}]^T$ is updated, and $\tilde{\mathbf{d}}_{\text{pre}}/\tilde{\mathbf{d}}_{\text{next}}$ are derived accordingly. Then the interference

Algorithm 1 Block-Wise Parallel Interference Cancellation (BwPIC)

Inputs: $\mathbf{y}$, Ψ_e, Ψ_{pre}, Ψ_{next}, I
output: $\tilde{\mathbf{d}}$
Initialization: $\tilde{\mathbf{d}} = \mathbf{0}_{\mathbf{KM}\times\mathbf{1}}$
for $i = 1; i <= I; i{+}{+}$ **do**
  $\tilde{\mathbf{d}}_{\text{pre}} = [\mathbf{0}_{M\times 1}, \tilde{\mathbf{d}}_1^T, \ldots, \tilde{\mathbf{d}}_{K-1}^T]^T$,
  $\tilde{\mathbf{d}}_{\text{next}} = [\tilde{\mathbf{d}}_2^T, \ldots, \tilde{\mathbf{d}}_K^T, \mathbf{0}_{M\times 1},]^T$
  $\hat{\mathbf{y}} = \mathbf{y} - \Psi_e\tilde{\mathbf{d}} - \Psi_{\text{pre}}\tilde{\mathbf{d}}_{\text{pre}} - \Psi_{\text{next}}\tilde{\mathbf{d}}_{\text{next}}$ (interference canceling)
  for $k = 1; k <= K; k{+}{+}$ **do**
    $\hat{\mathbf{d}}_k = \mathbf{E}\hat{\mathbf{y}}$ (one-tap equalization)
    $\tilde{\mathbf{d}}_k = \mathbb{Q}(\hat{\mathbf{d}}_k)$ (Slicing)
  end for
end for
return $\tilde{\mathbf{d}}_k$

corresponding to a whole block of f-OFDM symbols is canceled simultaneously according to (14) as

$$\hat{\mathbf{y}} = \mathbf{y} - \Psi_e\tilde{\mathbf{d}} - \Psi_{\text{pre}}\tilde{\mathbf{d}}_{\text{pre}} - \Psi_{\text{next}}\tilde{\mathbf{d}}_{\text{next}}; \tag{29}$$

however, the equalization and slicing are performed on a single f-OFDM symbol basis at each iteration of the inner loop. One-tap equalization is adopted in the algorithm for reducing computational complexity. The slicing operation approximates an equalized symbol to its nearest QAM point in the constellation.

IV. FILTER SELECTIVITY ANALYSIS AND DISCUSSION

In this section, we continue to investigate another issue (FFR selectivity), induced by the filtering operations in f-OFDM systems, which may cause system performance degradation.

An ideal low-pass filter is the one that completely eliminates all frequencies above a designated cutoff frequency, while leaving those below unchanged. Its frequency response is a rectangular function, as illustrated in red dotted line in Fig. 3. However, it is practically not possible to implement an ideal lowpass filter since the required impulse response is infinitely long. Practical filters have finite length, which inevitably leads to a nontrivial transition band between a passband and a stopband, as illustrated in the solid blue line in Fig. 3.

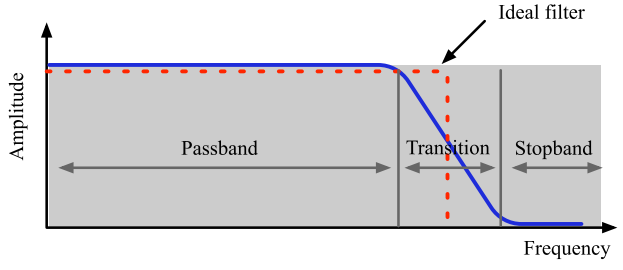

FIGURE 3. Ideal low-pass filters versus practical filters.

Filter selectivity refers to the frequency response in a transition band. It reduces the power of signals on the corresponding subcarriers which become undesirable for carrying data. As a result, the bandwidth efficiency is reduced. The bandwidth loss can be computed as bandwidth loss $= N_t/M$, where N_t is the number of subcarriers accommodated in the transition band, and M is the total number of subcarriers in the subband. This implies that the bandwidth loss increases linearly as the width of the subband decreases. Although the loss for medium/wide subband is not significant, for an extremely narrow subband with only one physical resource block (12 subcarriers), it reaches 33% when 4 subcarriers reside in the transition band. In terms of 5G mMTC service, aiming to provide a massive number of connections, the system band is expected to be divided into many narrow subbands. The bandwidth loss is severe in this case, which motivates us to consider exploiting these edge subcarriers to save the bandwidth. We will look into the issue in single antenna and multi-antenna systems respectively in the following subsections.

A. FILTER SELECTIVITY IN SINGLE ANTENNA SYSTEMS

We shall use the same system model described in Section II to investigate the issue caused by FFR selectivity in single antenna systems. Suppose the nearly interference-free condition defined in (25) is satisfied. After removing the CP/CS at the receiver, the FFT output, as the demodulated received signal on subcarrier $m \in \mathcal{M}$ in the k-th f-OFDM symbol, can be approximated according to (19) by

$$y_m = \ddot{p}_m\ddot{q}_m\ddot{h}_m d_m + \hat{w}_m, \tag{30}$$

where $\ddot{p}_m$, $\ddot{q}_m$, and $\ddot{h}$ are complex frequency responses of the transmitter filter, the receive filter, and the channel on subcarrier m, respectively. The subscript k as f-OFDM symbol index is dropped without loss of generality. Then, the average power of the desired signal on subcarrier m can be computed as

$$\tilde{\sigma}_{s,m}^2 = \mathcal{E}\{\ddot{p}_m\ddot{q}_m\ddot{h}_m d_m(\ddot{p}_m\ddot{q}_m\ddot{h}_m d_m)^*\} = |\ddot{p}_m\ddot{q}_m|^2\sigma_s^2$$

Due to the effect of FFR selectivity, the amplitude of frequency response of edge subcarriers is smaller than that of the middle subcarriers. Therefore, the power of received signal on edge subcarriers has a lower value than others, i.e., the probability that edge subcarriers go to deep fade increases, and the system performance degrades on these subcarriers. To tackle this issue, we proposed a pre-equalized f-OFDM system, denoted as pf-OFDM, in which, instead of directly modulating QAM complex symbols with equal powers on all subcarriers, we firstly precode the complex symbols with a weight defined as

$$g_m = \rho_{\text{pre-equ}}\frac{1}{\ddot{p}_m\ddot{q}_m^*}, \tag{31}$$

where $\rho_{\text{pre-equ}} < 1$ is power normalization factor to ensure the constant power before and after precoding. The precoding inverses the non-uniform distribution of filtering and eliminate FFR selectivity, as shown in Fig. 4. This enables that

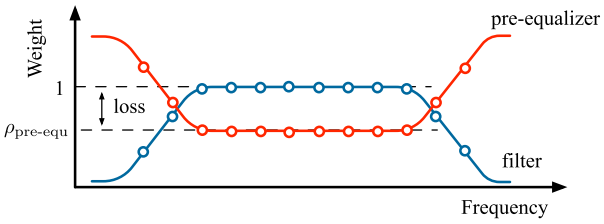

FIGURE 4. Illustration of pre-equalizer.

subcarriers in the transition band are able to carry data and avoids the bandwidth loss. However, this approach is not entirely free. It comes with a power loss of $\rho^2_{\text{pre-equ}}$, and the power normalization factor $\rho_{\text{pre-equ}}$ can be calculated as

$$\rho_{\text{pre-equ}} = \sqrt{\frac{M}{((\ddot{\mathbf{p}}.*\ddot{\mathbf{q}})^{-1})^H(\ddot{\mathbf{p}}.*\ddot{\mathbf{q}})^{-1}}}. \tag{32}$$

It is worth mentioning that $\rho_{\text{pre-equ}}$ is not a constant value but decreases as the width of subband grows, which indicates that narrower subbands suffer more power loss from pre-equalization.

B. FILTER SELECTIVITY IN MULTI-ANTENNA SYSTEMS

Spatial diversity, a well-known technique for combating the detrimental effects of multi-path fading, can be implemented either at the receiver side or the transmitter side. A space-time block code (STBC), referred as the Alamouti code after its inventor [28], has become the most popular means of achieving transmit diversity due to its ease of implementation (linear both at the transmitter and the receiver) and its optimality with regards to diversity order. Originally designed for a narrow band fading channel, STBCs can be easily adapted to wideband fading channel using OFDM by utilizing adjacent subcarriers rather than consecutive symbols, referred as space-frequency block code (SFBC). In SFBC-OFDM systems, the SFBC decoder can eliminate all spatial interference under the assumption that the channel is constant over two adjacent subcarriers. This is a reasonable assumption in OFDM systems if $B_c \gg B/N$, where B_c is channel coherence bandwidth, B is system bandwidth, and N is the number of subcarriers, which can be forced to be true by choosing a large enough number of subcarriers N. When SFBCs are implemented in f-OFDM systems (SFBC-f-OFDM), the FFR selectivity violates this condition and destroys the spatial orthogonality, which will be discussed in detail in the rest of the subsection.

For simplicity and consistency, we use a 2×1 Alamouti SFBC, but the concepts apply equally to any other higher dimensional transmit and receive antennas. Fig. 5 shows a block diagram of a generic filtered SFBC-OFDM system with two transmit antennas and a single receiver antenna. Assume that M subcarriers in the range of $\mathcal{M} = \{M_0, \ldots, M_0+M-1\}$ are assigned to a subband with a corresponding transmitter filter and receiver filter denoted as vector $\mathbf{p}$ and $\mathbf{q}$ in the time domain, respectively.

A block of data symbol $\mathbf{d} = (d_0, d_1, \ldots, d_{M-1})^T$ is fed into the SFBC encoder with the k-th sub-block orthogonal code in the form of

$$\mathbf{D}_k = \begin{bmatrix} d_{2k} & d_{2k+1} \\ -d^*_{2k+1} & +d^*_{2k} \end{bmatrix},$$

where $k = 0, 1, \ldots, M/2-1$, which generates two data sequences $\mathbf{d}^{(1)}, \mathbf{d}^{(2)}$ as $\mathbf{d}^{(1)} = [d_0, -d^*_1, d_2, -d^*_3, \ldots, d_{M-2}, -d^*_{M-1}]^T$, $\mathbf{d}^{(2)} = [d_1, +d^*_0, d_3, +d^*_2, \ldots, d_{M-1}, +d^*_{M-2}]^T$. The two data streams are pre-equalized by $M \times 1$ vector $\mathbf{g}$ before going through the IFFT / CP and filtering procedures independently as described in single-antenna systems, and they are then transmitted by the first and second antenna, respectively.

A flat fading channel is considered on each subcarrier. Denote the channel impulse response between transmit antenna i as $\mathbf{h}^{(i)} = [h^{(i)}_0, h^{(i)}_1, \ldots, h^{(i)}_{N^{(i)}_{\text{ch}}}]^T, i \in \{1, 2\}$, where each $h^{(i)}_n$ is a complex Gaussian random variable with zero mean and variance $\frac{1}{N^{(i)}_{\text{ch}}+1}$, and $\sum_{n=0}^{N^{(i)}_{\text{ch}}} \mathcal{E}\{|h^{(i)}_n|^2\} = 1$. $\ddot{h}^{(i)}_k = \sum_{n=0}^{N^{(i)}_{\text{ch}}} h^{(i)}_n e^{-j\frac{2\pi}{N}kn}$ corresponds to the DFT of $\mathbf{h}^{(i)}$ on the k-th subcarrier, and it is a complex Gaussian random variables with zero mean and variance one ($\mathcal{E}\{|\ddot{h}^{(i)}_k|^2\} = 1$). Assume that antennas at the transmitter are adequately apart so that channels are independent to each other, i.e., $\mathcal{E}\{\ddot{h}^{(1)}_k \ddot{h}^{(2)}_k\} = \mathcal{E}\{\ddot{h}^{(1)}_k\}\mathcal{E}\{\ddot{h}^{(2)}_k\}$.

Suppose that the length of CP/CS is chosen to ensure the nearly inference-free condition (25). After removing the CP/CS at the receiver, the FFT output, as the demodulated received signal vector, can be approximated according to (19) by

$$\mathbf{r} = \mathbf{QPH}^{(1)}\mathbf{Gd}^{(1)} + \mathbf{QPH}^{(2)}\mathbf{Gd}^{(2)} + \mathbf{Qv}, \tag{33}$$

where the $M \times 1$ vector $\mathbf{r} = (r_0, r_1, \ldots, r_{M-1})^T$. The $M \times M$ matrices $\mathbf{Q} = \text{diag}(\ddot{\mathbf{q}})$, $\mathbf{P} = \text{diag}(\ddot{\mathbf{p}})$, $\mathbf{H}^{(i)} = \text{diag}(\ddot{\mathbf{h}}^{(i)})$, $(i = 1, 2)$, $\ddot{\mathbf{p}}$, $\ddot{\mathbf{q}}$, $\ddot{\mathbf{h}}^{(i)}$, are filter frequency response vectors of the transmitter filter, the receiver filter and the channels over the subaband of interest. $\mathbf{v}_k$ is a length N Gaussian random vector with $\mathbf{v}_k \sim \mathcal{N}(\mathbf{0}_{M\times 1}, N_0\mathbf{I}_m)$.

Extracting the pair of received data symbols indexed at $2k, 2k+1$ from (33) gives

$$\begin{aligned} r_{2k} &= a^{(1)}_{2k} d_{2k} + a^{(2)}_{2k} d_{2k+1} + \ddot{q}_{2k} v_{2k} \\ r_{2k+1} &= -a^{(1)}_{2k+1} d^*_{2k+1} + a^{(2)}_{2k+1} d^*_{2k} + \ddot{q}_{2k+1} v_{2k+1} \end{aligned} \tag{34}$$

where $a^{(i)}_j = \ddot{h}^{(i)}_j \ddot{p}_j \ddot{q}_j g_j \quad i \in \{1, 2\},\ j \in \{2k, 2k+1\}$.

Assuming the channel and filtering information are perfectly known at the receiver, the following diversity combining scheme in the Alamouti SFBC decoder can be applied to give

$$\begin{bmatrix} \hat{d}_{2k} \\ \hat{d}_{2k+1} \end{bmatrix} = \begin{bmatrix} (a^{(1)}_{2k})^* & a^{(2)}_{2k+1} \\ (a^{(2)}_{2k})^* & -a^{(1)}_{2k+1} \end{bmatrix} \begin{bmatrix} r_{2k} \\ r^*_{2k+1} \end{bmatrix} \tag{35}$$

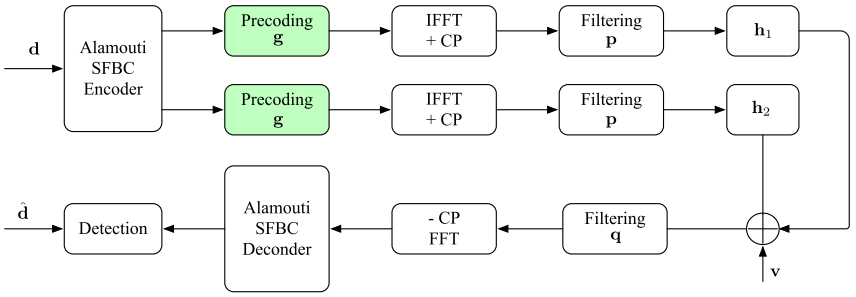

FIGURE 5. A block diagram of a generic filtered SFBC- OFDM system with two transmit antennas and a single receive antenna.

Substitute (34) into (35), we have

$$\begin{aligned}\hat{d}_{2k} &= \underbrace{(|a_{2k}^{(1)}|^2 + |a_{2k+1}^{(2)}|^2)d_{2k}}_{\text{desired signal}} + \underbrace{\beta_{2k}d_{2k+1}}_{\text{interference}} + \underbrace{w_{2k}}_{\text{noise}},\\ \hat{d}_{2k+1} &= \underbrace{(|a_{2k}^{(2)}|^2 + |a_{2k+1}^{(1)}|^2)d_{2k+1}}_{\text{desired signal}} + \underbrace{\beta_{2k+1}d_{2k}}_{\text{interference}} + \underbrace{w_{2k+1}}_{\text{noise}}, \quad (36)\end{aligned}$$

where

$$\begin{aligned}\beta_{2k} &= (a_{2k}^{(1)})^* a_{2k}^{(2)} - (a_{2k+1}^{(1)})^* a_{2k+1}^{(2)}\\ \beta_{2k+1} &= (a_{2k}^{(2)})^* a_{2k}^{(1)} - (a_{2k+1}^{(2)})^* a_{2k+1}^{(1)}\\ w_{2k} &= (a_{2k}^{(1)})^* \ddot{q}_{2k} v_{2k} + a_{2k+1}^{(2)} \ddot{q}_{2k+1}^* v_{2k+1}^*\\ w_{2k+1} &= (a_{2k}^{(2)})^* \ddot{q}_{2k} v_{2k} - (a_{2k+1}^{(1)})^* \ddot{q}_{2k+1}^* v_{2k+1}^*.\end{aligned}$$

The interference signals to d_{2k} and d_{2k+1} can be easily found from (36), and the average interference power to d_{2k} and d_{2k+1} can be computed as

$$\begin{aligned}\sigma_{\text{ini},2k}^2 &= \mathcal{E}\{\beta_{2k}d_{2k+1}(\beta_{2k}d_{2k+1})^*\} = \mathcal{E}\{\beta_{2k}\beta_{2k}^*\}\sigma_s^2,\\ \sigma_{\text{ini},2k+1}^2 &= \mathcal{E}\{\beta_{2k+1}d_{2k}(\beta_{2k+1}d_{2k})^*\} = \mathcal{E}\{\beta_{2k+1}\beta_{2k+1}^*\}\sigma_s^2.\end{aligned} \quad (37)$$

We assume that the channel is constant over the two adjacent subcarriers, i.e., $\ddot{h}_k^{(i)} = \ddot{h}_{k+1}^{(i)}$ $(i = 1, 2)$. Applying $\ddot{h}_k^{(i)} = \ddot{h}_{k+1}^{(i)}$ and substituting $a_j^{(i)} = \ddot{h}_j^{(i)}\ddot{p}_j\ddot{q}_j g_j$ into (37), yields

$$\begin{aligned}\sigma_{ini,2k}^2 = \sigma_{ini,2k+1}^2 = \big(&|\ddot{p}_{2k}|^2|\ddot{q}_{2k}|^2|g_{2k}|^2\\ &-|\ddot{p}_{2k+1}|^2|\ddot{q}_{2k+1}|^2|g_{2k+1}|^2\big)^2\sigma_s^2. \quad (38)\end{aligned}$$

Now, we divide the subcarrier set of interest $\mathcal{M}$ into two subsets: $\mathcal{M}_{\text{trans}}$ and $\mathcal{M}_{\text{pass}}$. Those subcarriers, locating in the passband, belong to the subset $\mathcal{M}_{pass}$, and the other subcarriers in the transition bands on both sides of the filter are grouped into the subset $\mathcal{M}_{trans}$. We will study the spatial orthogonality with respect to subcarriers of two subsets separately.

When both subcarriers $2k$ and $2k+1$ fall into the pass band region, the filter frequency response is constant. It gives

$$\begin{aligned}&|\ddot{p}_{2k}| = |\ddot{p}_{2k+1}|, |\ddot{q}_{2k}| = |\ddot{q}_{2k+1}| \text{ and } |g_{2k}| = |g_{2k+1}|,\\ &\qquad (M_{2k}, M_{2k+1} \in \mathcal{M}_{pass}). \quad (39)\end{aligned}$$

substituting (39) into (38) results in zero interference power, $\sigma_{ini,2k}^2 = \sigma_{ini,2k+1}^2 = 0$, and we have

Proposition 3: Proposition 3: The spatial orthogonality holds in SFBC-f-OFDM systems for those subcarriers in the passband region and the SNR is given as

$$\gamma_{2k} = \gamma_{2k+1} = \frac{|h_{2k}^{(1)}|^2 + |h_{2k}^{(2)}|^2}{\sigma_n^2}\frac{\sigma_s^2}{2}. \quad (40)$$

When at least one of the two subcarriers, either M_{2k} or M_{2k+1} resides in the region of the transition band, where FFR selectivity occurs, and we have

$$\begin{aligned}&|\ddot{p}_{2k}| \neq |\ddot{p}_{2k+1}| \text{ and } |\ddot{q}_{2k}| \neq |\ddot{q}_{2k+1}|\\ &\qquad (\forall (M_{2k}, M_{2k+1}) \in \mathcal{M}_{trans}). \quad (41)\end{aligned}$$

If no pre-equalization is implemented, $g_{2k} = g_{2k+1} = 1$, we have

Proposition 4: Proposition 4: The spatial orthogonality is destroyed in SFBC-f-OFDM systems for those subcarriers in the transition band region due to the FFR selectivity, and the non-trivial interference power is quantified as

$$\begin{aligned}\sigma_{ini,2k}^2 &= \sigma_{ini,2k+1}^2\\ &= \big(|\ddot{p}_{2k}|^2|\ddot{q}_{2k}|^2 - |\ddot{p}_{2k+1}|^2|\ddot{q}_{2k+1}|^2\big)^2\sigma_s^2. \quad (42)\end{aligned}$$

However, with the deployment of the pre-equalizer defined in (31) to reverse the effect of FFR selectivity, the interference across all subcarriers can be forced to zero, and we have

Proposition 5: Proposition 5: The spatial orthogonality holds in SFBC-pf-OFDM systems with the implementation of the per-equalizer defined in (31), and the SNR is given as

$$\gamma_{2k} = \gamma_{2k+1} = \frac{(|h_{2k}^{(1)}|^2 + |h_{2k}^{(2)})^2|)^2}{|h_{2k}^{(1)}|^2\ddot{q}_{2k}^2 + |h_{2k}^{(2)}|^2\ddot{q}_{2k+1}^2}\frac{\rho_{\text{pre-equ}}^2\sigma_s^2}{2\sigma_n^2}. \quad (43)$$

Comparing (43) to (40), it can be seen that the SNR loss due to the per-equalizer in SFBC-pf-OFDM systems is

$$\Gamma_{2k} = \frac{(|h_{2k}^{(1)}|^2 + |h_{2k}^{(2)})^2|)}{|h_{2k}^{(1)}|^2\ddot{q}_{2k}^2 + |h_{2k}^{(2)}|^2\ddot{q}_{2k+1}^2}\rho_{\text{pre-equ}}^2. \quad (44)$$

V. NUMERICAL RESULTS

In this section, we consider the evaluation of the following

1) the derived system model and interference power induced by filters with different settings,
2) the BER performance of f-OFDM single antenna systems under AWGN channels,[4] and the different performance enhancement techniques represented in Section III-D and Section IV-A,
3) the BER performance of f-OFDM/pf-OFDM multi-antenna systems under multi-path fading channels.

The following parameters, unless otherwise specified, are adopted for simulations. The f-OFDM system occupies $N = 1024$ subcarriers. The considered multi-path fading channel of length $N_f = 8$ is a block-fading Gaussian channel (BFGC), and the duration of a transmitted data block is smaller than the coherence time of the channel. Therefore, the fading envelope is assumed to be constant during the transmission of a block and independent from block to block. The length of a block (a frame) lasts over a duration of 14 OFDM symbols. It is assumed that the channel state information (CSI) is perfectly known at the receiver. A soft-truncated sinc filter defined in [14] is employed at the transmitter and receiver side, with filter length of $N_p = N_q = N/2$ and slope controlling parameters $\alpha_p = 0.6$, $\alpha_q = 0.65$.

A. NUMERICAL RESULTS FOR IN-BAND INTERFERENCE

The in-band interference in subsection III-A - III-C are numerically evaluated and plotted for different values in subband width and CR length.

Fig. 6 shows an example of power distributions for the desired signal and interference signal (ICI, forward ISI, and backward ISI) on a subcarrier level, evaluated through (22) with FFT size of 1024, subband width of 36 subcarriers in (a) and 240 subcarriers in (b). In addition, no CP/CS was added for interference alleviation. It is shown in the figure that the theoretical value of in-band interference power matches the simulation result. It is clearly visible that the interference in the wider subband have lower power as a whole than that of in the narrower band. Fig. 6 (a) indicates that uneven power is distributed for both the desired signal and interference signal among subcarriers. Comparing to other subcarriers, those near the edge (edge subcarriers) have lower desired signal power while experiencing higher interference. The two overlapping curves corresponding to the interference power from the previous f-OFDM (forward ISI) and next f-OFDM symbol (backward ISI) indicates the same power distribution due to the symmetry of the filters. The trends are also captured in Fig. 6 (b) for the wider subband.

The maximum, minimum, and average normalized power of ICI/ISI with respect to subcarriers of the same subband are shown in Fig. 7, where the ISI represents forward ISI or backward ISI as both have the same power distribution indicated

[4]The reason that AWGN channels are chosen for verifying BER performance is to rule out the impact of the multi-path fading channel and focus on the interference produced by filtering.

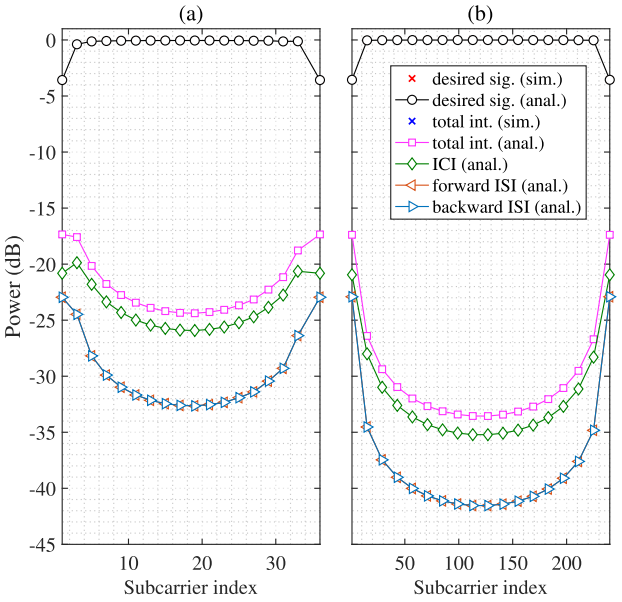

FIGURE 6. Power of desired signal and interference $N = 1024$, $N_{cr} = 0$, $N_p = N_q = 512$, $\alpha_p = 0.6$, $\alpha_q = 0.65$. The three contributions (ICI, forward ISI, and backward ISI) to the total interference are evaluated individually from our analytical expressions, which can not be fulfilled through simulation, thus only the analytical results of them are plotted. (a) a narrow subband of 3 RBs (36 subcarriers). (b) a wider subband of 20 RBs (240 subcarriers).

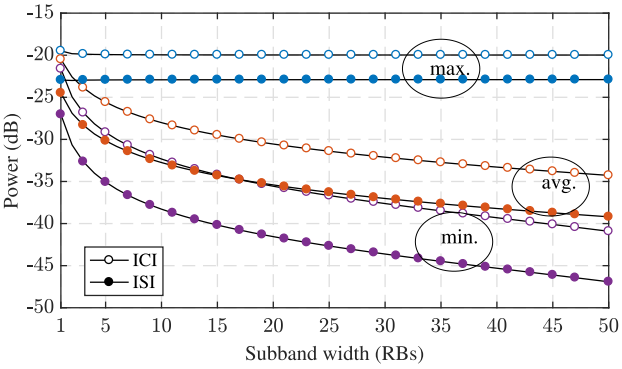

FIGURE 7. Max, min, and average normalized power of ICI/ISI with respect to subcarriers against subbands of different width with $N = 1024$, $N_{cr} = 0$, $N_p = N_q = 512$, $\alpha_p = 0.6$, $\alpha_q = 0.65$, ISI represents either forward ISI or backward ISI. All curves of the figure are generated from the analytical results.

in Fig. 6. These results provide a direct comparison among subbands with varying width from 1 RB to 50 RBs. It can be seen that the maximum normalized power keeps constant as the width of subband grows. However, this is not the case with the minimum and average normalized power, where both decrease as the subband width increase. This implies that narrower subbands are more prone to in-band interference compared to wider subbands. These features apply to both the ICI and ISIs.

Fig. 8 presents the average effective interference power of six subbands of variable width versus the number of CRs, where $N_{cp} = N_{cs} = N_{cr}/2$. The effective interference here

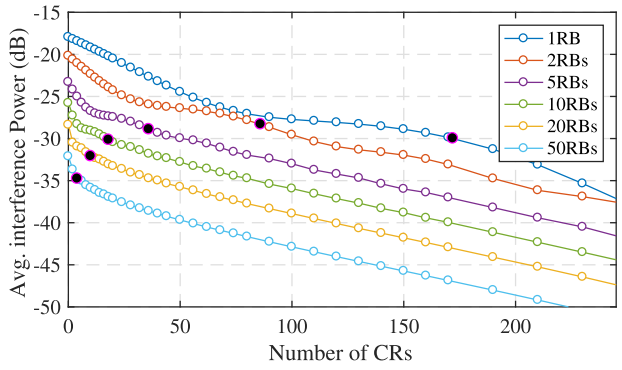

FIGURE 8. Average effective interference power with respect to subcarriers vs. number of CRs with $N = 1024$, $N_{cr} = 0$, $N_p = N_q = 512$, $\alpha_p = 0.6$, $\alpha_q = 0.65$, the solid black dots indicate the number of CRs equals the width of the filter main lobe of the corresponding subband. All curves of the figure are generated from the analytical results.

refers to the sum of the ICI, forward and backward ISI. The effect of CR length for alleviating in-band interference is observed from all these curves. The power of the average effective interference decreases as the length of CR increases, and it drops under 25 dB for all six subbands when the number of CRs equals to the length of corresponding filter main lobe due to the fact that most of the filter energy is contained in the main lobe.

The BER performance of f-OFDM under the AWGN channel is evaluated and plotted in Fig. 9. The results are presented in two cases, $N_{cr} = 0$ in (a) and $N_{cr} = 72$ in (b), each having six curves corresponding to a different subband width and a curve representing the BER of legacy OFDM for a benchmark comparison. Taking into the consideration of computational complexity at the receiver side, one-tap equalization method

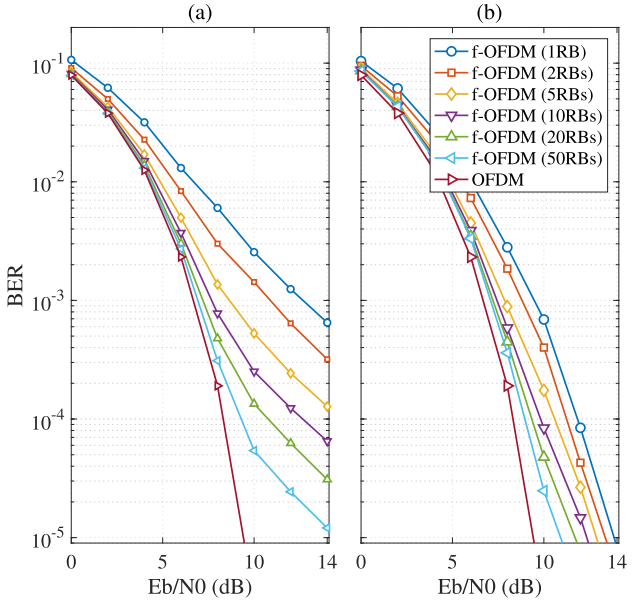

FIGURE 9. Error performance for f-OFDM systems under AWGN channel with QPSK modulation. (a) $N_{cp} = N_{cs} = 0$. (b) $N_{cp} = N_{cs} = 36$.

is adopted. When the in-band interference is not handled by introducing CR, the performance of f-OFDM, as shown in Fig. 9(a), degrades dramatically comparing with OFDM systems. Moreover, error floors also tend to develop for all subbands. Another interesting observation is that the performance degradation in narrower subbands is higher than that of in the wider subbands, again suggesting that narrower subbands suffer more in-band interference. In (b), the BER performance is significantly improved due to the use of the CR. There is still a gap of approximately 2-5 dB, subject to how wide the subband of interest is, which implies that there is still space to improve, especially for narrow subbands.

The effect of different approaches to interference suppression is shown in terms of BER performance enhancement in Fig. 10 with two different CR length setting, $N_{\rm cr} = 0$ and $N_{\rm cr} = 24$ in a subband of 12 subcarriers. It can be seen that ZF and MMSE have almost the same BER performance in both CR settings. However, the BER performance with the implementation of BwPIC improves significantly compared to the systems without BwPIC, and the results also show that the algorithm converges with no more than two iterations.

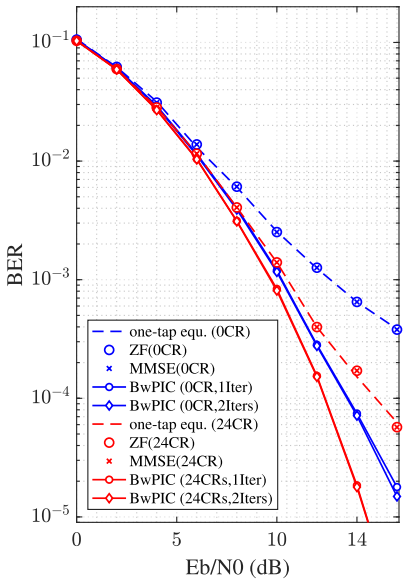

FIGURE 10. Error performance comparison with and without implementation of BwPIC for f-OFDM systems under AWGN channels with QPSK modulation.

B. NUMERICAL ANALYSIS FOR FILTER SELECTIVITY

Fig. 11 plots the interference power for an SFBC-f-OFDM system without the pre-equalization obtained in (42). The result shows that the interference increases as the difference in filter gain between two subcarriers grows, implying that the system suffers more interference in a region with higher filter selectivity.

The BER performance of f-OFDM in single and multiple antenna systems is numerically evaluated under the AWGN and multi-path fading channel respectively. In the case of single antenna systems, we use the same simulation parameters chosen in V-A so that the performance with and without

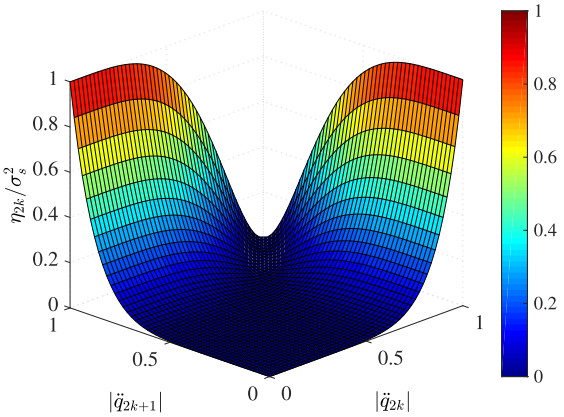

FIGURE 11. Interference power (normalized by signal power) versus filter frequency responses of consecutive subcarriers.

pre-equalization can be compared fairly. Fig. 12 compares the BER performance of f-OFDM systems with and without pre-equalization, and it can be clearly seen that pf-OFDM outperforms f-OFDM for all subbands. It is also observed that the BER performance of pf-OFDM is very close to OFDM when the width of the subband is over 5 RBs. Although there is still some gap for the narrower subbands, the performance is considerably improved in comparison to that of f-OFDM without pre-equalization. The remaining performance gap to OFDM systems can be explained by the power loss due to the pre-equalization.

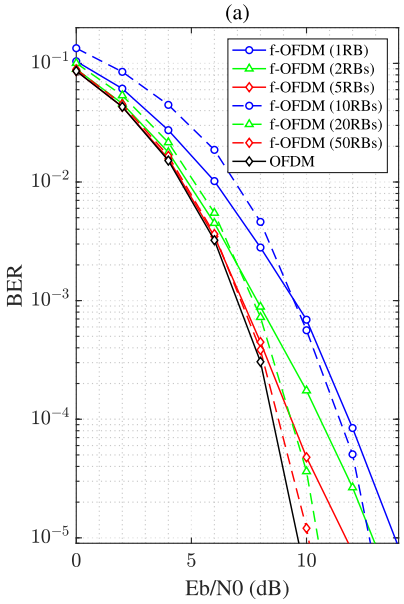

FIGURE 12. Error performance comparison with and without implementation of pre-equalization under AWGN channels with QPSK modulation.

The BER performance of SFBC-OFDM is numerally evaluated and plotted in Fig. 13 for different values of subband width without and with pre-equalization. It can be seen from the figure that SFBC-pf-OFDM dramatically

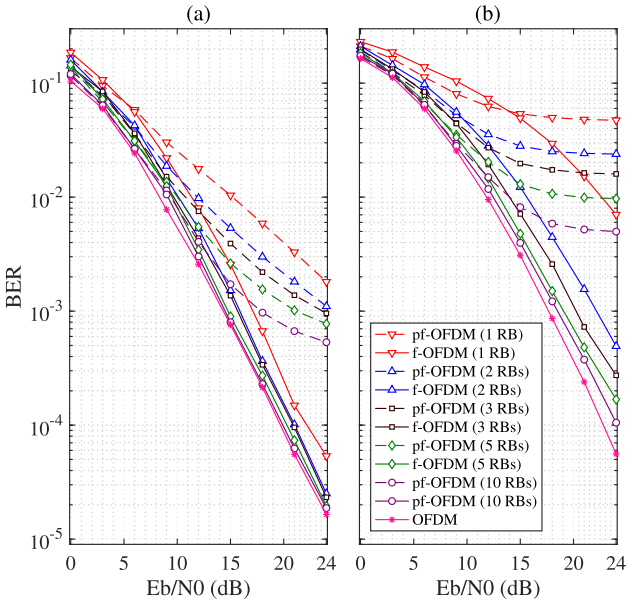

FIGURE 13. BER performance for filtered SFBC-OFDM systems with and without pre-equalization under Rayleigh fading channel with $N = 1024, N_p = N_q = 512, \alpha_p = 0.6, \alpha_q = 0.65$. (a) QPSK. (b) 16-QAM.

outperform SFBC-f-OFDM, and as the width of subband grows, the BER performance converges to the benchmark result of SFBC-OFDM. The effect of different modulation scheme is also observed from these curves, and the BER performance of QPSK is better than 16-QAM as expected. In the case of 16-QAM, error floors are quickly developed due to the interference introduced by spatial non-orthogonality in SFBC-f-OFDM without pre-equalization systems, implying that it cannot be implemented when higher modulation schemes are adopted. However, error floors do not exist in SFBC-pf-OFDM with pre-equalization systems as the spatial orthogonality is protected from being destroyed by the FFR selectivity.

VI. CONCLUSION

This paper modeled a single subband matrix-form f-OFDM system, in which all the linear convolution operations were converted into matrix multiplications to derive a well-channelized signal. Based on this model, the analytical expressions of the in-band interference, including ICI, forward ISI, and backward ISI, were derived, and the interference-free condition was developed. In addition, we proposed a low-complexity FEQ algorithm - BwPIC to cancel the in-band interference. Furthermore, the effect of FFR selectivity to single antenna and multi-antenna f-OFDM systems was discussed, and a pre-equalization approach was proposed to tackle it. As the simulation results show, our analytical interference power calculated from analytical expression matches the simulation results, validating the analytical model established in this paper. The proposed BwPIC effectively cancels the interference signal and significantly improves the BER performance. With the proposed equalizer,

pf-OFDM outperforms f-OFDM and is close to OFDM in single antenna systems. In contrast, in multi-antenna systems, it protects spatial orthogonality from destruction by the FFR selectivity. To conclude, the work presented in this paper provides a useful reference and valuable guidance for the practical deployment of the waveform in future wireless systems.

APPENDIX A
DERIVATION OF $\mathbf{z}_k$

Substituting $\mathbf{r}_k$ in equ. (12) with its expression in (9), followed by replacing $\mathbf{s}_k$ with its expression in (5), we obtain

$$\begin{aligned}\mathbf{z}_k = &(\mathbf{Q}^u\mathbf{H}^m + \mathbf{Q}^m\mathbf{H}^u)(\mathbf{P}^u\mathbf{x}_{k-2} + \mathbf{P}^m\mathbf{x}_{k-1} + \mathbf{P}^l\mathbf{x}_k)\\ &+(\mathbf{Q}^m\mathbf{H}^m + \mathbf{Q}^l\mathbf{H}^u)(\mathbf{P}^u\mathbf{x}_{k-1} + \mathbf{P}^m\mathbf{x}_k + \mathbf{P}^l\mathbf{x}_{k+1})\\ &+\mathbf{Q}^l\mathbf{H}^m(\mathbf{P}^u\mathbf{x}_k + \mathbf{P}^m\mathbf{x}_{k+1} + \mathbf{P}^l\mathbf{x}_{k+2})\\ &+\tilde{\mathbf{w}}_k,\end{aligned} \tag{45}$$

where $\tilde{\mathbf{w}}_k = \mathbf{Q}^u\mathbf{w}_{k-1} + \mathbf{Q}^m\mathbf{w}_k + \mathbf{Q}^l\mathbf{w}_{k+1}$ is the filtered AWGN signal.

To simplify (45) and eliminate redundant terms, we introduce the following properties:

1) The product of the two strictly upper triangular matrices is zero, and the product of the two strictly lower triangular matrices is also zero.
2) The product of $\mathbf{P}^u/\mathbf{Q}^u$ and $\mathbf{H}^m$ is a strictly triangular matrix $\mathbf{A}$ with $\mathbf{A}_{i,j} = 0$, when $i > j - [L - \frac{N_p}{2} - (N_{\text{ch}} - 1)]$. The proof can be found in Appendix C.

We have $\mathbf{Q}^u\mathbf{H}^u = 0$ under the Property 1), $\mathbf{Q}^u\mathbf{H}^m\mathbf{P}^u = 0$ and $\mathbf{Q}^l\mathbf{H}^m\mathbf{P}^l = 0$ under the Property 1) and 2), thus obtaining a simplified version of $\mathbf{z}_k$

$$\mathbf{z}_k = \Theta_{\text{pre}}\mathbf{x}_{k-1} + \Theta\mathbf{x}_k + \Theta_{\text{next}}\mathbf{x}_{k+1} + \tilde{\mathbf{w}}_k, \tag{46}$$

where $\Theta_{\text{pre}} = \mathbf{Q}^u\mathbf{H}^m\mathbf{P}^m + \mathbf{Q}^m\mathbf{H}^u\mathbf{P}^m + \mathbf{Q}^m\mathbf{H}^m\mathbf{P}^u$, $\Theta = \mathbf{Q}^u\mathbf{H}^m\mathbf{P}^l + \mathbf{Q}^m\mathbf{H}^u\mathbf{P}^l + \mathbf{Q}^m\mathbf{H}^m\mathbf{P}^m + \mathbf{Q}^l\mathbf{H}^u\mathbf{P}^m + \mathbf{Q}^l\mathbf{H}^m\mathbf{P}^u$, and $\Theta_{\text{next}} = \mathbf{Q}^m\mathbf{H}^m\mathbf{P}^l + \mathbf{Q}^l\mathbf{H}^u\mathbf{P}^l + \mathbf{Q}^l\mathbf{H}^m\mathbf{P}^m$.

APPENDIX B
PROOF OF Θ_{pre} BEING A STRICT UPPER TRIANGLE

As $\Theta_{\text{pre}} = (\mathbf{Q}^u\mathbf{H}^m\mathbf{P}^m + \mathbf{Q}^m\mathbf{H}^m\mathbf{P}^u + \mathbf{Q}^l\mathbf{H}^u\mathbf{P}^u)$. Following the same approach in Appendix C, we can prove the following: 1) the product of $\mathbf{Q}^u\mathbf{H}^m\mathbf{P}^m$ is a strictly upper triangular matrix of which only the top $\frac{N_p}{2}$ rows have non-zero elements, 2) the product of $\mathbf{Q}^m\mathbf{H}^u\mathbf{P}^m$ is a strictly upper triangular matrix of which only the top $\frac{N_p}{2} + N_{\text{ch}}$ rows have non-zero elements, 3) the product of $\mathbf{Q}^m\mathbf{H}^m\mathbf{P}^u$ is a strictly upper triangular matrix of which only the top $N_p + N_{\text{ch}}$ rows have non-zero elements. Therefore, the sum of three strictly upper triangular matrices results in a strictly upper triangular matrix Θ_{pre}, and only the top $N_p + N_{\text{ch}}$ rows of it have non-zero elements.

APPENDIX C
PROOF OF PROPERTY 2)

The product of $\mathbf{P}^u/\mathbf{Q}^u$ and $\mathbf{H}^m$ is a strictly triangular matrix $\mathbf{A}$, with $A_{i,j} = 0$, when $i > j - [L - \frac{N_p}{2} - (N_{\text{ch}} - 1)]$. As $\mathbf{P}^u$ and $\mathbf{Q}^u$ are matrices with the same structure, we will only give the detailed steps for proving one of them. The other one can be done in the similar fashion.

$$\begin{aligned}A_{i,j} &= \sum_{k=1}^{L} {P^u}_{i,k}{H^m}_{k,j}\\ &= \sum_{k=1}^{j+N_{\text{ch}}-1} {P^u}_{i,k}{H^m}_{k,j} + \sum_{k=j+N_{\text{ch}}}^{L} {P^u}_{i,k}{H^m}_{k,j}\end{aligned} \tag{47}$$

Because the condition $i > j - [L - \frac{N_p}{2} - (N_{\text{ch}} - 1)]$, when $1 \le k \le j + N_{ch} - 1$, we have

$$\begin{aligned}k - (L - \frac{N_p}{2}) \le k \le j + N_{ch} - 1 - (L - \frac{N_p}{2}) < i\\ \Rightarrow k < i + L - \frac{N_p}{2}\end{aligned} \tag{48}$$

and this gives ${P^u}_{i,k} = 0$ according to (6). Therefore, the first term of (47),

$$\sum_{k=1}^{j+N_{\text{ch}}-1} {P^u}_{i,k}{H^m}_{k,j} = 0.$$

When $j + N_{\text{ch}} \le k \le L$, we have ${H^m}_{k,j} = 0$ based on (10). Therefore, the second term of (47), $\sum_{k=j+N_{\text{ch}}}^{L} {P^u}_{i,k}{H^m}_{k,j} = 0$, is also proved.

As a result, $A_{i,j} = 0$ is proved, because both its sum terms in (47) equal to zero, when $i > j - [L - \frac{N_p}{2} - (N_{\text{ch}} - 1)]$.

REFERENCES

[1] P. Banelli, S. Buzzi, G. Colavolpe, A. Modenini, F. Rusek, and A. Ugolini, "Modulation formats and waveforms for 5G networks: Who will be the heir of OFDM?: An overview of alternative modulation schemes for improved spectral efficiency," *IEEE Signal Process. Mag.*, vol. 31, no. 6, pp. 80–93, Nov. 2014.
[2] G. Wunder, P. Jung, M. Kasparick, T. Wild, F. Schaich, Y. Chen, S. Brink, I. Gaspar, N. Michailow, A. Festag, L. Mendes, N. Cassiau, D. Ktenas, M. Dryjanski, S. Pietrzyk, B. Eged, P. Vago, and F. Wiedmann, "5GNOW: Non-orthogonal, asynchronous waveforms for future mobile applications," *IEEE Commun. Mag.*, vol. 52, no. 2, pp. 97–105, Feb. 2014.
[3] B. Farhang-Boroujeny, "OFDM versus filter bank multicarrier," *IEEE Signal Process. Mag.*, vol. 28, no. 3, pp. 92–112, May 2011.
[4] R. Razavi, P. Xiao, and R. Tafazolli, "Information theoretic analysis of OFDM/OQAM with utilized intrinsic interference," *IEEE Signal Process. Lett.*, vol. 22, no. 5, pp. 618–622, May 2015.
[5] N. Michailow, M. Matthé, I. S. Gaspar, A. N. Caldevilla, L. L. Mendes, A. Festag, and G. Fettweis, "Generalized frequency division multiplexing for 5th generation cellular networks," *IEEE Trans. Commun.*, vol. 62, no. 9, pp. 3045–3061, Sep. 2014.
[6] J. Zhong, G. Chen, J. Mao, S. Dang, and P. Xiao, "Iterative frequency domain equalization for MIMO-GFDM systems," *IEEE Access*, vol. 6, pp. 19386–19395, 2018.
[7] L. Zhang, P. Xiao, and A. Quddus, "Cyclic prefix-based universal filtered multicarrier system and performance analysis," *IEEE Signal Process. Lett.*, vol. 23, no. 9, pp. 1197–1201, Sep. 2016.
[8] A. A. Zaidi, J. Luo, R. Gerzaguet, A. Wolfgang, R. J. Weiler, J. Vihriala, T. Svensson, Y. Qi, H. Halbauer, Z. Zhao, P. Zetterberg, and H. Miao, "A preliminary study on waveform candidates for 5G mobile radio communications above 6 GHz," in *Proc. IEEE 83rd Veh. Technol. Conf. (VTC Spring)*, May 2016, pp. 1–6.
[9] L. Zhang, A. Ijaz, P. Xiao, and R. Tafazolli, "Multi-service system: An enabler of flexible 5G air interface," *IEEE Commun. Mag.*, vol. 55, no. 10, pp. 152–159, Oct. 2017.
[10] J. Abdoli, M. Jia, and J. Ma, "Filtered OFDM: A new waveform for future wireless systems," in *Proc. IEEE 16th Int. Workshop Signal Process. Adv. Wireless Commun. (SPAWC)*, Jun. 2015, pp. 66–70.

[11] X. Zhang, M. Jia, L. Chen, J. Ma, and J. Qiu, "Filtered-OFDM-enabler for flexible waveform in the 5th generation cellular networks," in *Proc. IEEE Global Commun. Conf. (GLOBECOM)*, Dec. 2015, pp. 1–6.
[12] P. Xiao, C. Toal, D. Burns, V. Fusco, and C. Cowan, "Transmit and receive filter design for OFDM based WLAN systems," in *Proc. Int. Conf. Wireless Commun. Signal Process. (WCSP)*, Oct. 2010, pp. 1–4.
[13] J. Li, K. Kearney, E. Bala, and R. Yang, "A resource block based filtered OFDM scheme and performance comparison," in *Proc. ICT*, May 2013, pp. 1–5.
[14] D. Wu, X. Zhang, J. Qiu, L. Gu, Y. Saito, A. Benjebbour, and Y. Kishiyama, "A field trial of F-OFDM toward 5G," in *Proc. IEEE Globecom Workshops (GC Wkshps)*, Dec. 2016, pp. 1–6.
[15] P. Guan, X. Zhang, G. Ren, T. Tian, A. Benjebbour, Y. Saito, and Y. Kishiyama, "Ultra-low latency for 5G–a lab trial," 2016, *arXiv:1610.04362*. [Online]. Available: http://arxiv.org/abs/1610.04362
[16] P. Weitkemper, J. Bazzi, K. Kusume, A. Benjebbour, and Y. Kishiyama, "On regular resource grid for filtered OFDM," *IEEE Commun. Lett.*, vol. 20, no. 12, pp. 2486–2489, Dec. 2016.
[17] P. Guan, D. Wu, T. Tian, J. Zhou, X. Zhang, L. Gu, A. Benjebbour, M. Iwabuchi, and Y. Kishiyama, "5G field trials: OFDM-based waveforms and mixed numerologies," *IEEE J. Sel. Areas Commun.*, vol. 35, no. 6, pp. 1234–1243, Jun. 2017.
[18] J. Yli-Kaakinen, T. Levanen, S. Valkonen, K. Pajukoski, J. Pirskanen, M. Renfors, and M. Valkama, "Efficient Fast-Convolution-Based waveform processing for 5G physical layer," *IEEE J. Sel. Areas Commun.*, vol. 35, no. 6, pp. 1309–1326, Jun. 2017.
[19] L. Zhang, A. Ijaz, P. Xiao, M. M. Molu, and R. Tafazolli, "Filtered OFDM systems, algorithms, and performance analysis for 5G and beyond," *IEEE Trans. Commun.*, vol. 66, no. 3, pp. 1205–1218, Mar. 2018.
[20] X. Wang, T. Wild, F. Schaich, and S. ten Brink, "Pilot-aided channel estimation for universal filtered multi-carrier," in *Proc. IEEE 82nd Veh. Technol. Conf. (VTC-Fall)*, Sep. 2015, pp. 1–5.
[21] D. Demmer, R. Gerzaguet, J.-B. Doré, D. Le Ruyet, and D. Ktenas, "Block-filtered OFDM: A novel waveform for future wireless technologies," in *Proc. IEEE Int. Conf. Commun. (ICC)*, May 2017, pp. 1–6.
[22] *NR; Base Station (BS) Radio Transmission and Reception*, document TS 38.104, 3GPP, Sep. 2019.
[23] L. Zhang, A. Ijaz, P. Xiao, A. Quddus, and R. Tafazolli, "Subband filtered multi-carrier systems for multi-service wireless communications," *IEEE Trans. Wireless Commun.*, vol. 16, no. 3, pp. 1893–1907, Mar. 2017.
[24] B. Sklar and F. J. Harris, *Digital Communications: Fundamentals and Applications*. Englewood Cliffs, NJ, USA: Prentice-Hall, 1988.
[25] K. Cho and D. Yoon, "On the general BER expression of one- and two-dimensional amplitude modulations," *IEEE Trans. Commun.*, vol. 50, no. 7, pp. 1074–1080, Jul. 2002.
[26] J. G. Andrews, "Interference cancellation for cellular systems: A contemporary overview," *IEEE Wireless Commun*, vol. 12, no. 2, pp. 19–29, Apr. 2005.
[27] T. Manglayev, R. C. Kizilirmak, and Y. H. Kho, "Comparison of parallel and successive interference cancellation for non-orthogonal multiple access," in *Proc. Int. Conf. Comput. Netw. Commun. (CoCoNet)*, Aug. 2018, pp. 74–77.
[28] S. M. Alamouti, "A simple transmit diversity technique for wireless communications," *IEEE J. Sel. Areas Commun.*, vol. 16, no. 8, pp. 1451–1458, Oct. 1998.

JUQUAN MAO received the B.Eng. degree in computer science and technology from Qingdao University, China, in 2003, the M.Sc. degree in computer science and technology from the Beijing University of Posts and Telecommunications, China, in 2006, and the Ph.D. degree in electrical and electronic engineering from the University of Surrey, U.K., in 2019. He was a Technical Engineer with Huawei Technologies Company, Ltd., from 2006 to 2012. He was a Lecturer with the Department of Electrical Engineering, London South Bank University, U.K., from 2012 to 2016. He is currently a Research Fellow with 5GIC, Faculty of Engineering and Physical Sciences, University of Surrey. His main interests include 5G new waveforms and mixed numerology, physical layer network slicing, and nonorthogonal multiple access.

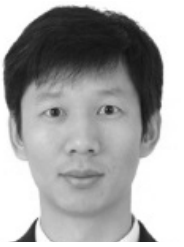

LEI ZHANG (Senior Member, IEEE) received the Ph.D. degree from The University of he field, U.K. He is currently a Lecturer with the University of Glasgow, U.K. He has 19 U.S./U.K./EU/China granted/filed patents on wireless communications and published two books and more than 100 peer-reviewed articles. His research interests include wireless communications and networks, blockchain, radio access network slicing (RAN slicing), the Internet of Things (IoT), multiantenna signal processing, MIMO systems, and so on. He received the IEEE Communication Society TAOS Best Paper Award, in 2019. He was the Publication and Registration Chair of the IEEE Sensor Array and Multichannel (SAM) 2018, the Publicity Chair of 4th U.K.- China Emerging Technologies (UCET) 2019, and the Co-Chair of the Cyber-C Blockchain Workshop 2019. He is an Associate Editor of the IEEE INTERNET OF THINGS (IoT) JOURNAL, the IEEE WIRELESS COMMUNICATIONS LETTERS, and the IEEE ACCESS.

PEI XIAO (Senior Member, IEEE) is currently a Professor of wireless communications with the Institute for Communication Systems, Home of 5G Innovation Centre (5GIC), University of Surrey. He is the Technical Manager of 5GIC, leading the research team in the new physical layer work area, and coordinating/supervising research activities across all the work areas within 5GIC. Prior to this, he worked at Newcastle University and Queen's University Belfast. He also held positions at Nokia Networks in Finland. He has published extensively in the fields of communication theory, RF and antenna design, and signal processing for wireless communications. He is an inventor on over ten recent 5GIC patents addressing bottleneck problems in 5G systems.

KONSTANTINOS NIKITOPOULOS (Senior Member, IEEE) is currently an Associate Professor in signal processing for communication systems with the Institute for Communication Systems, University of Surrey, Guildford, U.K., and a member of the 5G Innovation Centre (5GIC). He is the Director of the newly established "Wireless Systems Laboratory." He also leads the "Theory and Practice of Advanced Concepts in Communications" Work Area in 5GIC. He has held research positions with RWTH Aachen University, the University of California at Irvine, and the University College London. He was a recipient of the prestigious First Grant of the U.K.'s Engineering and Physical Sciences Research Council and the Principal Investigator of several research projects, including AutoAir, a UK funded project on "5G Testbeds and Trials." He has been a consultant for the Hellenic General Secretariat for Research and Technology, where he has also served as a National Delegate of Greece to the Joint Board on Communication Satellite Programs of European Space Agency.